JOURNAL OF PROPULSION AND POWER
Vol. 19, No. 2, March–April 2003

Axial Compressor Blade-to-Blade Unsteady Aerodynamic Variability

Douglas M. Boyd* and Sanford Fleeter†
Purdue University, West Lafayette, Indiana 47907

Experiments investigate axial compressor unsteady aerodynamics generated by the interaction of rotor blades with the wakes from inlet guide vanes (IGVs). The variability of the unsteady velocity and the corresponding unsteady aerodynamic rotor blade response are determined. The percentage of IGV wakes similar to the grand average wake is calculated in and out of wake-affected regions. Also, the probability distributions of wake characteristics are made, and the correlation between the forcing function and the response variability calculated. Significant blade-to-blade variability is found, with less than 50% of the wakes similar to the grand average percentage. The energy in the unsteadiness varies by as much as 100%. A strong correlation between the transverse velocity and the resulting unsteady aerodynamic response is found. However, the correlation weakens at lower flow coefficients due to stall on the suction surface of the IGV.

Nomenclature

C_l = lift coefficient
C_M = moment coefficient
T_{BP} = blade passing period
wc = wake width characteristic
w_τ = transverse gust component
w_ψ = streamwise gust component
Π = compressor pressure rise coefficient
τ = direction normal to the steady rotor relative velocity
ψ = direction parallel to the steady rotor relative velocity

Subscript

gr = grand average

Superscripts

$\bar{\ }$ = time averaged
Λ = ensemble averaged

Introduction

CURRENT models to predict the unsteadiness in turbomachinery consider only the blade pass frequency and higher harmonics. Thus, these models assume that all airfoils produce identical wakes and respond to unsteadiness in the exactly same manner. However, no two wakes are ever identical. Hence, the goal of this study is to investigate blade-to-blade wake and resulting unsteady aerodynamic response variability. Sources of this variability include manufacturing differences, stagger and spacing variances, and blade row interactions.

The limited work done with blade-to-blade wake variability has shown it to be significant. Sherman et al.[1] studied the pressure behind an axial compressor rotor and computed a grand mean wake by averaging the wakes from each rotor blade. They found that the number of wakes that can be represented by a grand mean wake varies in and out of the wake region. About 50% of the wakes were considered to not be represented by the grand mean. Sanders and Fleeter[2] quantified wake variability for a rotor wake and the resulting unsteady lift of the downstream stator. At the design condition, the variability of the velocity deficit was about 13% of the maximum deficit, and the unsteady lift coefficient varied by about 50%. At an off-design condition, the variability increased due to flow separation on the rotor.

Experimental Methods

The compressor test section has inlet guide vanes (IGVs) and two stages of rotor blades and stator vanes with a C4 profile and a 30-mm chord. The axial spacing between the IGVs and first rotor is 72.0% chord and 296% chord between the first stage rotor and the next stator. Also, support struts (3.3 mm thick and 98 mm long) are located 84 mm upstream of the test section.

The rotor-based instrumentation is shown in Fig. 1. Two-dimensional velocity measurements are accomplished with a rotating TSI 1240-T1.5 cross hot wire capable of accurate measurements to 200 kHz. The hot wire is located at midspan, 18.8% chord upstream and 17.4% blade spacing circumferentially from the nearest rotor blade and is calibrated for velocities from 21 to 61 m/s and angles to ±36 deg. The first stage rotor blade unsteady static pressures are measured using 20 Kulite XCS-093-2A transducers at midspan, with four blades used due to space limitations. A dynamic transducer calibration determined that the maximum gain error was 0.60 dB and phase angle was 1.5 deg from 40 to 2700 Hz.

Data Analysis

The velocity and blade surface unsteady pressure signals are sampled at 100 kHz, with 606,000 samples taken corresponding to over 200 rotor revolutions with 3000 points each and the ensemble average $\hat{z}(j)$ and ensemble standard deviation $\hat{z}_\sigma(j)$ calculated. The crosswire and the four unsteady surface pressure blades are at different rotor locations. Hence, the ensemble average signals are shifted in time to simulate one rotor location. To determine if wakes are like a grand average,[1] first the 3000-point ensemble averaged data signal is divided into 36 random vectors $\boldsymbol{X}_i$ corresponding to the 36 IGV wakes. Because there are 3000 points and 36 wakes per revolution, there are 83.333 points per wake, that is, not a whole number. Therefore, only 83 points are taken for each wake with one point skipped every third wake. A difficulty arises from the interaction of the five upstream support struts with the IGVs. The five affected IGV wakes are not used in the variability analysis, leaving 31 random vectors for variability analysis.

The variability analysis determines whether the variability of the 31 IGV wakes is due only to a statistical variation. The estimates

Received 16 January 2001; revision received 2 October 2002; accepted for publication 10 November 2002.

*Graduate Research Assistant, School of Mechanical Engineering; currently Project Engineer, System Performance, Rolls–Royce Corporation. Member AIAA.

†McAllister Distinguished Professor, School of Mechanical Engineering. Fellow AIAA.

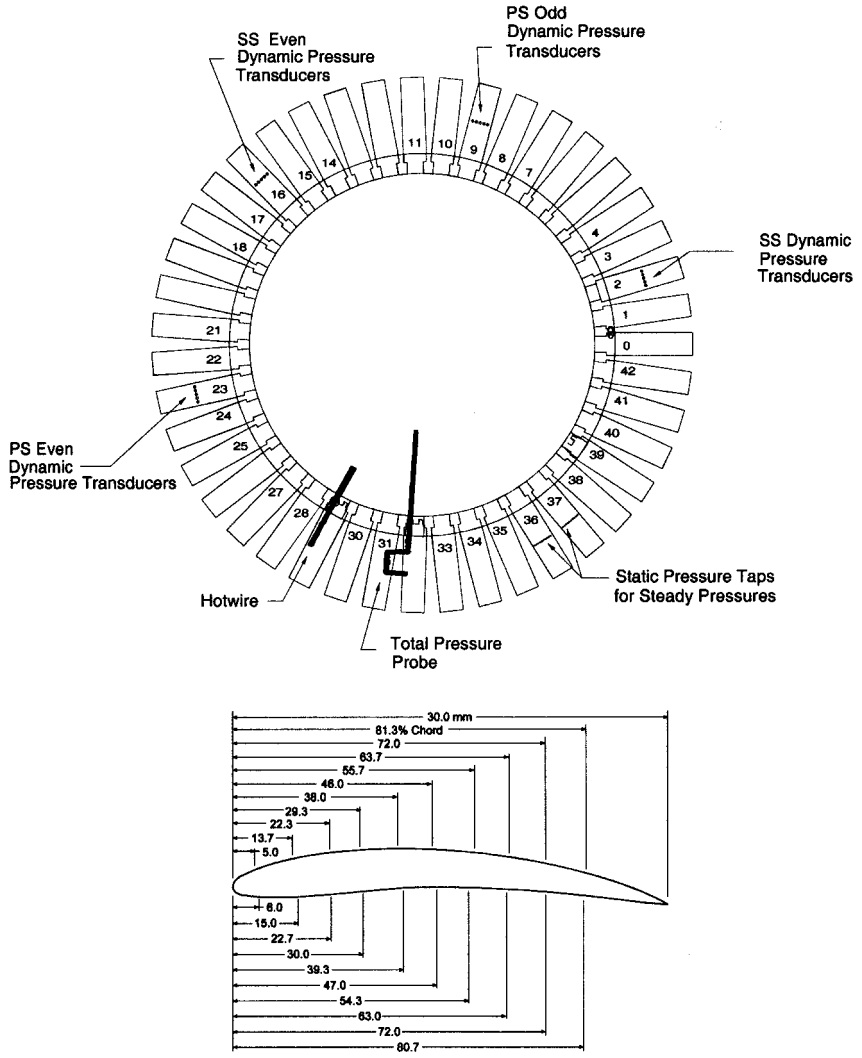

Fig. 1 Rotor-based instrumentation.

of the ensemble standard deviations $\hat{z}_\sigma$ calculated in the ensemble averaging are divided into 31 random vectors $\boldsymbol{Y}_i$ as were the ensemble averages. Also, grand average and grand standard deviation vectors from the 31 wakes are calculated [Eq. (1)]. The grand average specifies the average wake, with the standard deviation quantifying the difference between the individual wakes and the grand average:

$$\boldsymbol{X}_{\mathrm{gr}}(j) = \frac{1}{N_{\mathrm{wakes}}} \sum_{i=1}^{N_{\mathrm{wakes}}} \boldsymbol{X}_i(j)$$

$$\boldsymbol{Y}_{\mathrm{gr}}(j) = \sqrt{\frac{1}{N_{\mathrm{wakes}'}} \sum_{i=1}^{N_{\mathrm{wakes}'}} [\boldsymbol{X}_i(j) - \boldsymbol{X}_{\mathrm{gr}}(j)]^2} \qquad (1)$$

where N_{wakes} is the number of wakes used to make the grand average (31).

The Smith–Satterthwaite test compares two independent random samples that are assumed to be from normal distributions with unequal variances and is used to compare each of the 83 points of the grand average and the individual wake ensemble averages [Eq. (2)]. The degrees of freedom and test statistics are calculated for each point of each wake. Finally, for each of the 83 points of the wake ensembles, the fraction of wake ensembles that can be represented by the grand average wake ensemble is calculated. A high fraction (>0.71) means the grand average is a good representation of the wakes and the wake-to-wake variability is due to chance:

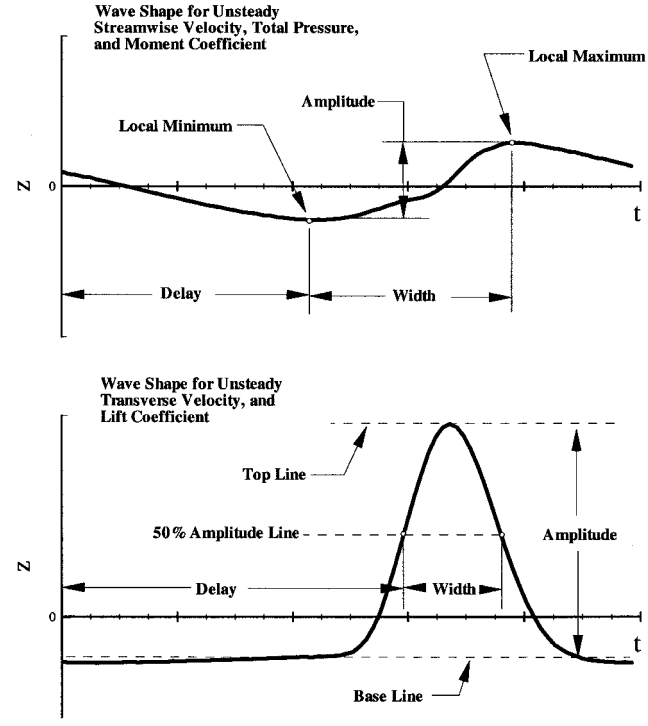

Fig. 2 Wake shapes.

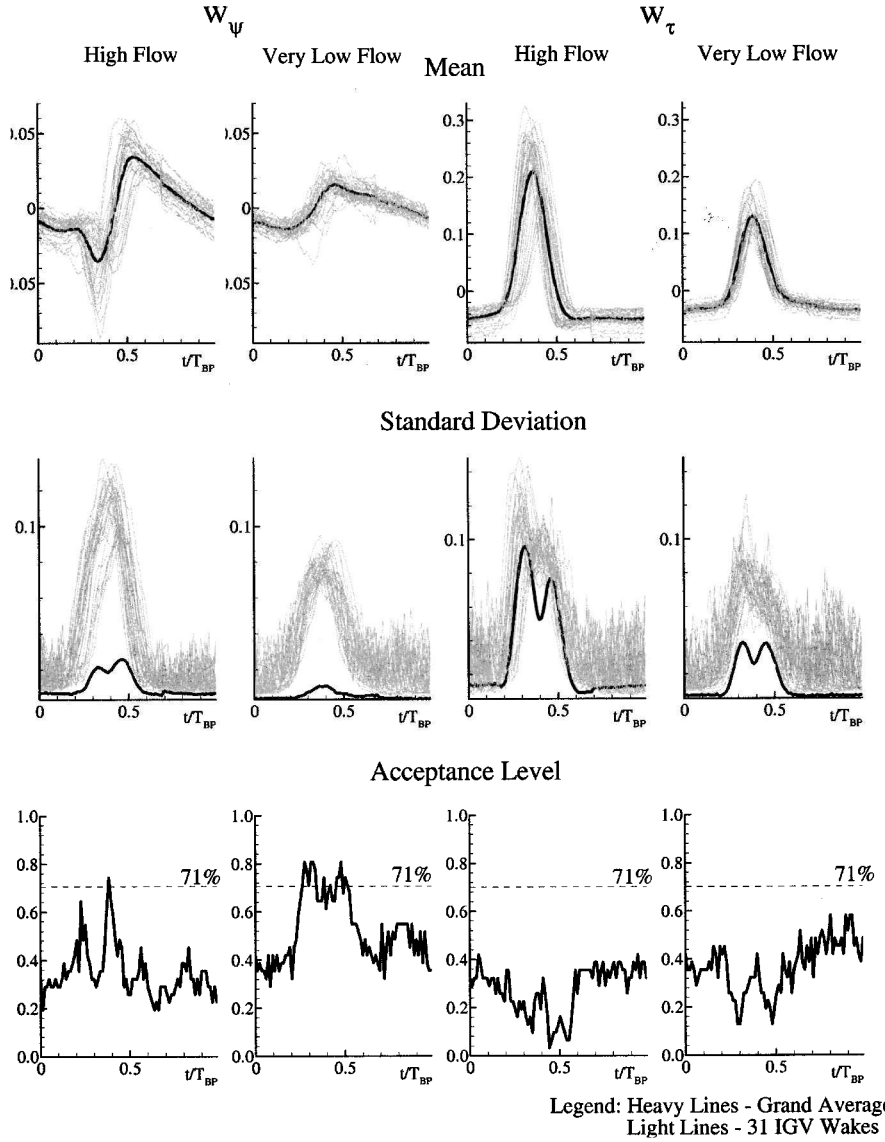

Fig. 3 Forcing function mean, standard deviation, and acceptance levels.

$$D_i(j) = \left(\frac{\boldsymbol{Y}_i(j)}{N_{\text{rev}}} + \frac{\boldsymbol{Y}_{\text{gr}}(j)}{N_{\text{wakes}'}}\right)^2 \Bigg/ \left\{\frac{[\boldsymbol{Y}_i(j)/N_{\text{rev}}]^2}{N_{\text{rev}}-1} + \frac{[\boldsymbol{Y}_{\text{gr}}(j)/N_{\text{wakes}'}]^2}{N_{\text{wakes}'}-1}\right\}$$

$$t_i(j) = |\boldsymbol{X}_i(j) - \boldsymbol{X}_{\text{gr}}(j)| \Bigg/ \sqrt{\frac{\boldsymbol{Y}_i(j)^2}{N_{\text{rev}}} + \frac{\boldsymbol{Y}_{\text{gr}}(j)^2}{N_{\text{wakes}}}} \tag{2}$$

where $D_i(j)$ is the number of degrees of freedom of the jth point in the ith wake, $t_i(j)$ is the test statistic of the jth point in the ith wake, N_{rev} is the number of revolutions used in the ensemble average (200), and $N_{\text{wakes}'}$ is the number of wakes used to make the grand average wake (31).

The variability is further examined by quantifying the wake characteristic distributions. The streamwise and transverse velocities are again used for the forcing function, with the unsteady lift and moment coefficients used for the rotor blade response. The four characteristics analyzed are the delay, width, amplitude, and energy of the wake or response. The delay is the time between the start of the time trace and a set event. Width is a measure of how long the wake effect lasts. Amplitude defines the peak-to-peak change caused by the wake. The energy is a measure of the total unsteadiness, quantified by the sum of the square of the unsteady signal.

The characteristic values are corrected by the grand average characteristic. The corrected delay is calculated by subtracting the grand average delay from each of the wake delays with the difference divided by the blade passing period, that is, the corrected delay is the difference from the grand mean delay as a fraction of the blade pass period. The corrected width, amplitude, and energy are calculated similarly, but the difference from the mean is divided by the grand average. The corrected amplitude and energy are calculated in the same manner. A corrected value of zero means that the width of a wake is equal to the width of the grand average. A corrected value of one means the width of a wake is twice that of the grand average.

To find if the blade-to-blade variability of the unsteady aerodynamic response is related to that of the forcing function, the correlation coefficient is calculated,

$$\text{correlation coefficient} = \frac{N}{N-1}\frac{\text{cov}(wc_{\text{ff}}, wc_{\text{res}})}{\sqrt{\text{cov}(wc_{\text{ff}}, wc_{\text{ff}}) \cdot \text{cov}(wc_{\text{res}}, wc_{\text{res}})}} \tag{3}$$

where the covarience

$$\text{cov}(a,b) = \frac{1}{N}\sum_i a_i b_i - \frac{1}{N^2}\sum_i a_i \sum_i b_i$$

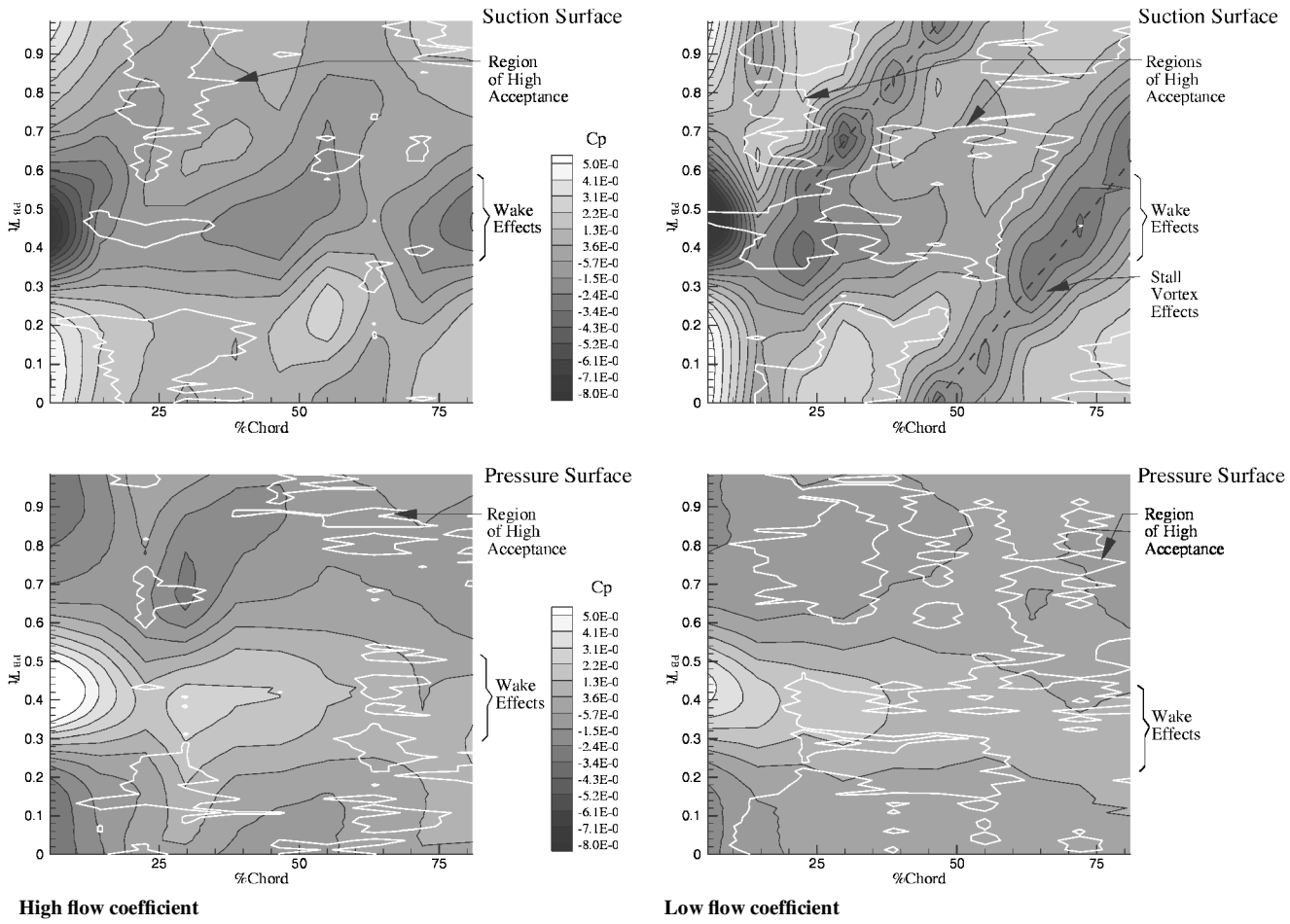

High flow coefficient **Low flow coefficient**

Fig. 4 Grand average aerodynamic blade response and acceptance level.

Once the wake-to-wake variability due to chance has been determined, the variability can be further examined by quantifying the distribution of the wake characteristics. The streamwise and transverse velocities are again used as the forcing function signals. However, for the rotor blade response, the unsteady lift and moment coefficients are analyzed. There are two types of wake shapes for these signals, as shown in Fig. 2. One type is similar to an impulse, whereas the other is similar to a sinusoidal wave. The transverse gust and unsteady lift have impulse shapes whereas the streamwise gust and unsteady moment have sinusoidal variations.

The four wake characteristics analyzed are the delay, width, amplitude, and energy of the wake or response. The delay is the time between the start of the time trace and a set event. Width is a measure of how long the wake effect lasts. Amplitude is a measure of the peak-to-peak change caused by the wake. For pulse shaped signals, the American National Standards Institute/Institute of Electrical and Electronics Engineers 194-1977 standard for pulse terms and definitions is used. The sinusoidal signals are analyzed by determining local maximums and minimums caused by the wake. The energy is a measure of the total unsteadiness and is found by taking the sum of the square of the unsteady signal.

Results and Discussion

The blade-to-blade variabilities at the high and very low flow coefficients on a constant-speed operating cure are compared herein. The acceptance testing is applied to two forcing function parameters, streamwise velocity w_ψ and transverse velocity w_τ, with Fig. 3 showing the degree of unsteadiness vs the fraction of the rotor blade pass period. Figure 3 shows the 31 ensemble average wakes as light lines and the grand mean wake as the dark line. Note that the streamwise unsteady velocity is much smaller. The standard deviation plot shows the 31 ensemble average standard deviations and the grand average standard deviation.

The 31 w_ψ ensemble averages follow the same trend as the grand average; however, the location and magnitude of the local maximum changes. The 31 ensemble standard deviations have a maximum, whereas the velocity is changing from the highest to lowest point that is in the wake region. For the high flow coefficient, the grand average standard deviation has two local maximums that correspond to the minimum and maximum of the grand average mean. As the flow coefficient is lowered, the grand average standard deviation decreases. The resulting acceptance level is generally higher in the wake region than in the freestream. The maximum acceptance, above 71%, occurs during a short time in the wake region for the high flow coefficient and even longer for the very low flow coefficient. In the freestream, the acceptance is 20–40% with the lower flow coefficient having higher acceptance.

The 31 w_τ ensemble averages have larger unsteadiness than w_ψ. All 31 wakes form a positive pulse in the wake region, with the pulse amplitude decreasing with flow coefficient. The ensemble average standard deviations have two local maximums that correspond to the maximum and minimum of the ensemble averages. The ensemble average standard deviation decreases with flow coefficient. The grand average standard deviations also have two local maximums that decrease with flow coefficient. For w_τ, the acceptance is lower in the wake region, opposite from w_ψ. In the wake region, the acceptance has two local minimums at the beginning and end of the wake with a maximum in the middle. In the freestream, the acceptance levels are generally higher at the low flow coefficient.

All 20 of the surface unsteady pressures are acceptance tested, analogous to the forcing function. The grand average pressures across the suction and pressure surfaces are shown in Fig. 4. Regions

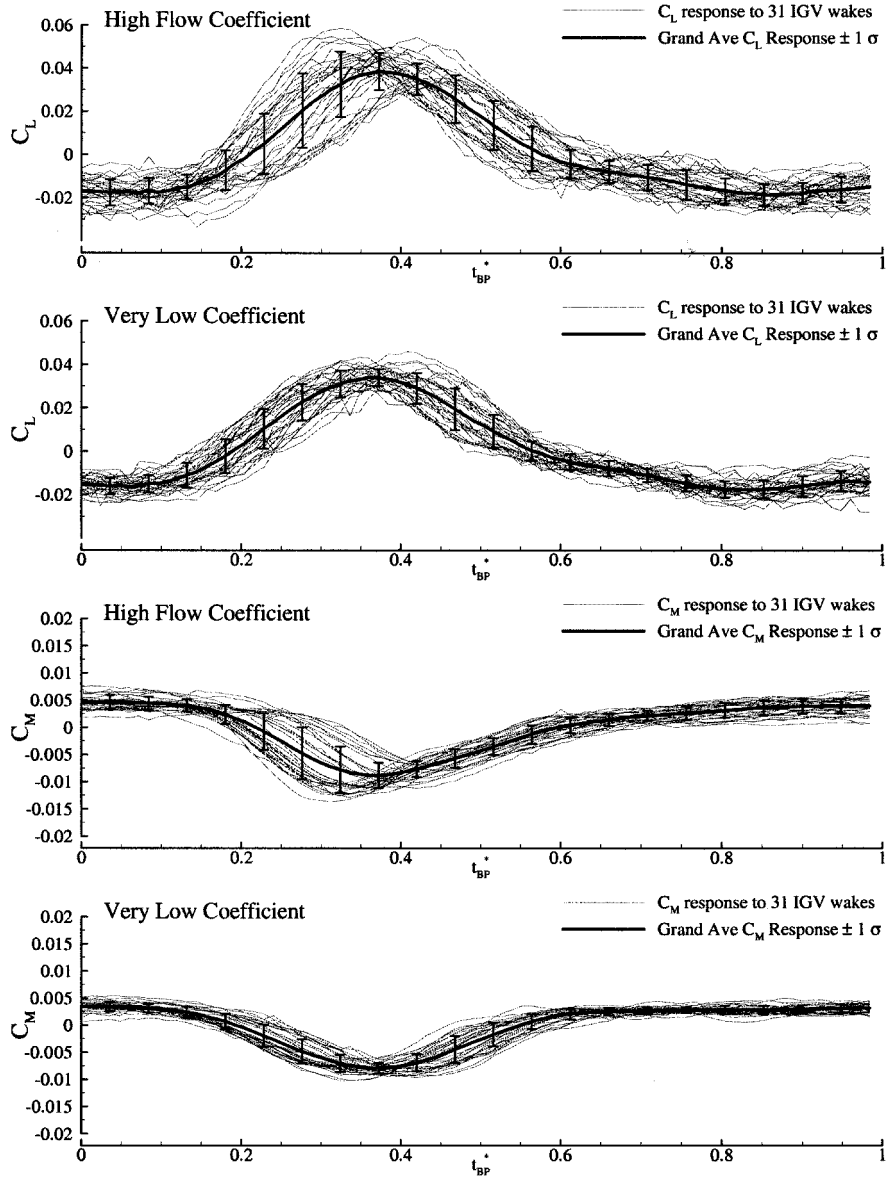

Fig. 5 Unsteady lift and moment coefficient from 31 IGV wakes and the grand average.

with acceptance above 71% are outlined by white lines. As shown by the large unsteadiness, the IGV wake is on the rotor blade from about 0.25 to $0.45t/T_{BP}$. On the suction surface, the wake causes a negative pressure shown by the dark color, whereas on the pressure surface, the wake increases the pressure and, thus, the color is light.

On the rotor blade suction surface, the regions of high acceptance change with flow coefficient. At the high flow condition, the high acceptance region is present from 20 to 35% chord at the beginning and end of the wake-affected region. At the low flow condition, the other high acceptance region develops aft of the stall vortex. The stall vortex is shown by a negative pressure than goes from about 25% chord to the trailing edge during the blade pass period. Before the vortex reaches a part of the rotor blade, there is a region of high acceptance. This is likely due to the high ensemble standard deviation that is a result of the stall vortex having an inconsistent formation and propagation rate. On the pressure surface, the high acceptance is concentrated in regions unaffected by the wake. At the high flow coefficient, high acceptance is present between 20 and 30% chord except when the wake is present and between 60 and 75% chord. These high acceptance regions grow with lower flow coefficient. At the very low flow coefficient, there is high acceptance for all but the front 10% chord.

Because blade-to-blade wake variability was found in both the forcing function and unsteady aerodynamic response, the distribution of the wake characteristic is of interest. For the forcing function, the unsteady streamwise and transverse velocities are again examined, with the unsteady lift and moment used as a summary of the rotor unsteady suction and pressure surface pressures (Fig. 5). Shown are the 31 ensemble responses, the grand average and its standard deviation. The 31 ensemble responses vary more that one standard deviation from the grand average. However, the blade-to-blade variability decreases with lower flow coefficients.

The wake characteristic probability distributions are shown in Fig. 6. The delay is predominantly within ±20 and ±10% of the IGV/rotor blade pass period for the high and very low flow coefficients. The width of the velocity wake coefficients is very consistent, especially at the low flow condition. The amplitude characteristics have more variance than the width characteristics. The w_ψ amplitude has a broad distribution of ±60% of the mean. The w_τ amplitude distribution has many values within 20% of the mean, with the whole distribution within ±40% of the mean. The w_ψ energy is distributed evenly and broadly over ±100% of the mean value. The distribution for the w_τ energy is slightly smaller. Therefore these high-energy variance values indicate that the blade-to-blade wake variability is significant.

The characteristic distributions for the unsteady lift and moment coefficients are shown in Fig. 7. The delays of the unsteady lift and moment have similar distributions. The delay distributions become

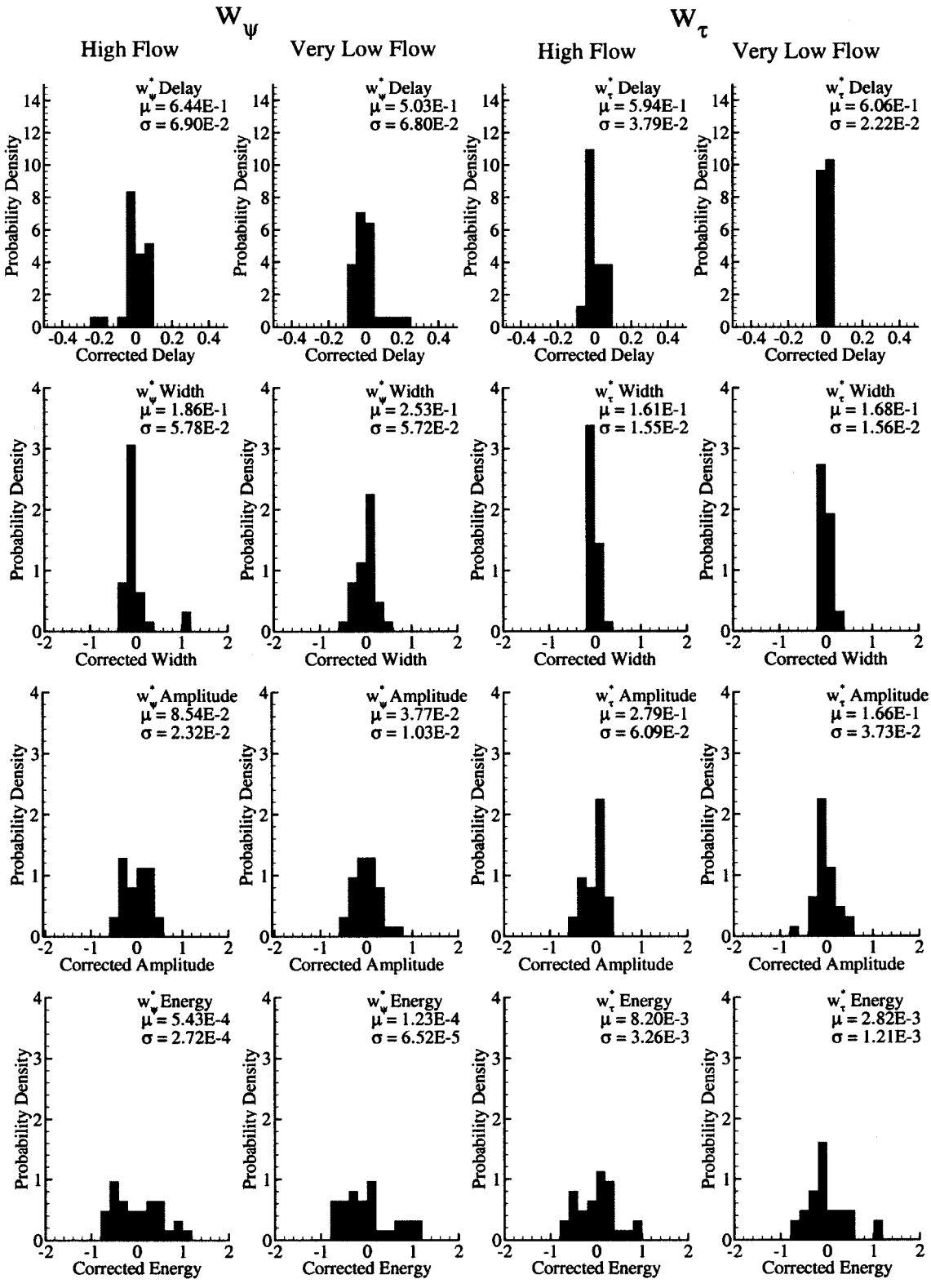

Fig. 6 Forcing function wake characteristic probability distributions.

narrower with lower flow coefficient. The distributions of the width characteristic for the unsteady lift and moment are very different. The width of the unsteady lift coefficient varies within ±100% of the mean. Conversely, the width of the unsteady moment coefficient only varies ±20% for all flow coefficients. The amplitude distributions of the unsteady lift and moment coefficients are similar, staying within ±50% of the mean. The variance is lower at the very low standard flow coefficient than at the high flow coefficient. The energy of the unsteady lift and moment coefficients stays within 60% of the mean value for both flow coefficients. Even though the unsteady lift and moment coefficients are calculated by integration, these results show significant blade-to-blade variance.

Both the forcing function and unsteady aerodynamic response contain significant blade-to-blade variability. Because the forcing function is the primary source for the unsteadiness of the unsteady aerodynamic response, there should be a correlation between them. However, some of the unsteady response is due to the interaction of the forcing function and the rotor blades, such as the formation of the

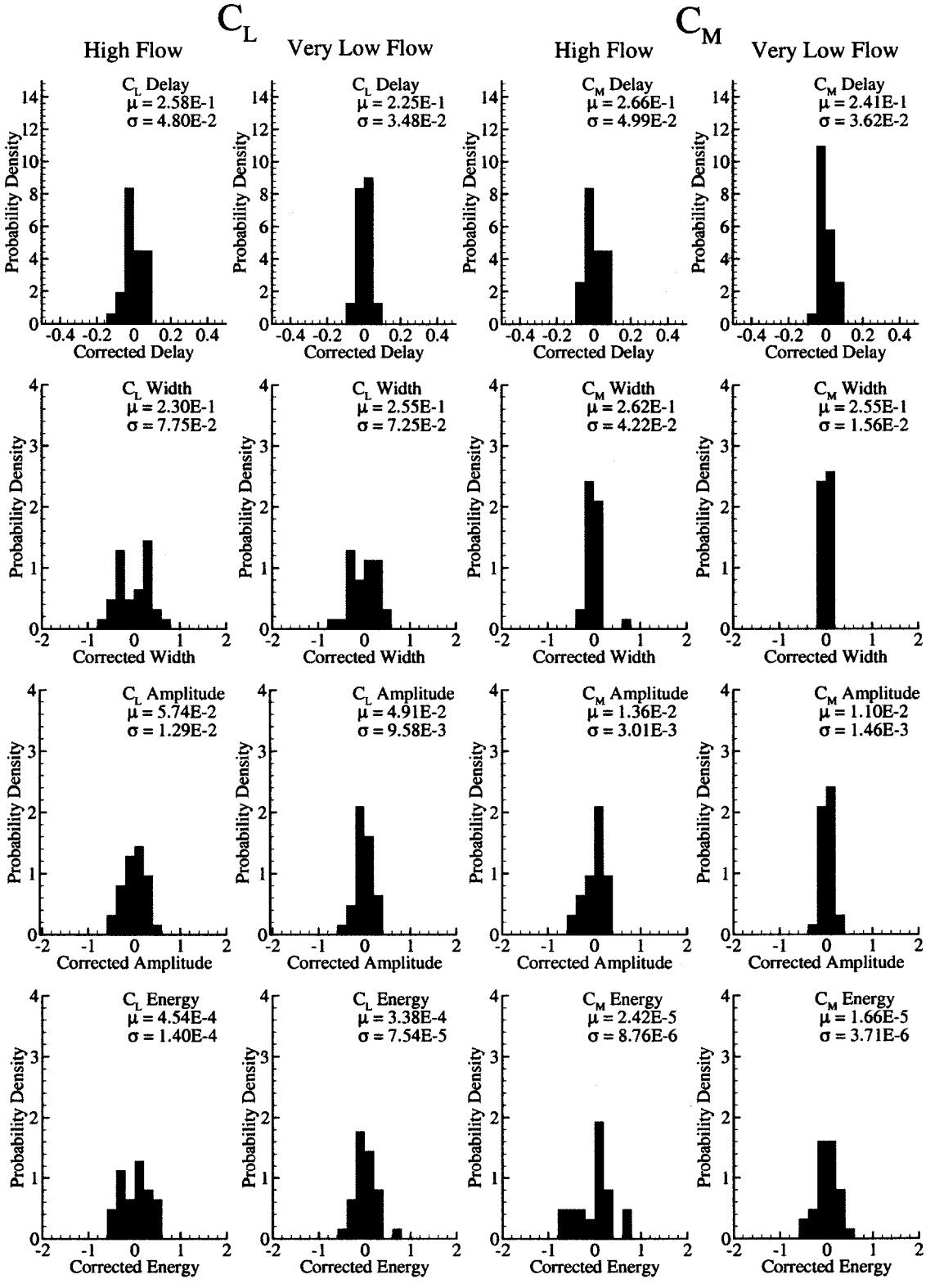

Fig. 7 Lift and moment characteristic probability distributions.

stall vortex. Therefore, there may be some variability in the response not present in the forcing function. To measure the forcing function and aerodynamic response correlation, the correlation coefficient is calculated between each of the forcing function characteristics and the response characteristics.

The delay characteristic shows a strong relation between the transverse velocity and unsteady aerodynamic response. Between the delay of the transverse unsteady velocity and that of the unsteady lift, the correlation coefficient decreases from 0.90 at the high flow condition to 0.65 at the very low flow coefficient. The correlation coefficient between the delay of the transverse velocity and the unsteady moment also decreases, but only from 0.94 to 0.81. These high correlations show that the timing of the unsteady blade response is closely tied to that of the unsteady transverse velocity. However, this relation decreases at the lower flow coefficients, indicating other factors are affecting the response, for example,

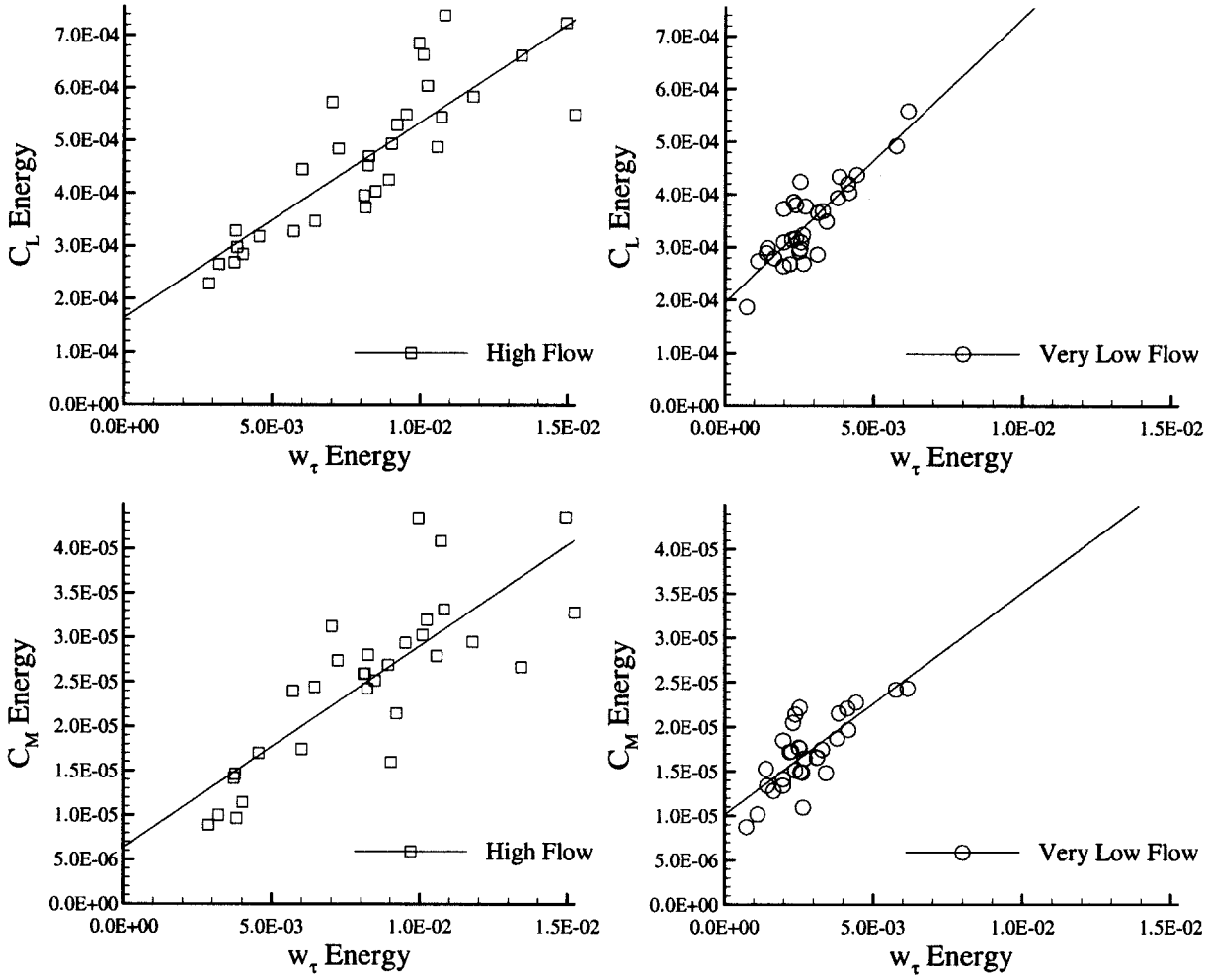

Fig. 8 Unsteady lift and transverse velocity energy characteristic relation.

suction surface stall. The energy characteristic also shows a strong relation between the transverse velocity and the unsteady lift. The correlation coefficients between them are 0.85 and 0.86. Therefore, the amount of unsteadiness in the transverse velocity is closely related to the responding unsteady lift. These characteristics are plotted in Fig. 8 and show the linear relationship.

The correlation coefficients between the energy of the transverse velocity and the unsteady moment are also strong, 0.81 and 0.77 for the four flow coefficients. The lower correlation values at the lower flow coefficients indicate that the energy in the unsteady moment coefficient becomes less dependent on the transverse velocity. This lack of correlation is likely due to the stall vortex effects that become a significant influence on the unsteady moment coefficient at low flow conditions. Notice that, at the low flow condition, there is a weaker relationship between the transverse velocity and the unsteady moment coefficient.

Summary

Experiments investigated axial compressor unsteady aerodynamics generated by the interaction of rotor blades with the wakes from IGVs. The vane-to-vane variability of the rotor inlet unsteady velocity and the corresponding unsteady aerodynamic response of the rotor blade row were determined. The percentage of wakes similar to the grand average IGV wake was calculated in and out of wake-affected regions. Also, the probability distributions of wake characteristics were made, and the correlation between the forcing function and the resulting unsteady aerodynamic response variability was calculated.

Blade-to-blade variability of the forcing function and resulting unsteady aerodynamic response was significant. The streamwise unsteady velocity has low blade-to-blade variability in the wake region, but not in the freestream. Conversely, the transverse unsteady velocity is like the grand average in the freestream and not in the wake. On the suction surface, the response blade-to-blade variability is low except in wake and stall vortex-affected regions. The response on the pressure surface is like the grand average. The characteristic of the wakes and response vary by as much as 100%. The forcing function and response characteristics show a strong correlation between the transverse velocity and the unsteady lift coefficient for both the timing and the amount of unsteady energy. The correlation between the transverse velocity and the unsteady moment coefficient decreases significantly for the very low flow coefficient due to the effects of blade stall. In summery, blade-to-blade variability can lead to variability in the unsteady aerodynamic response, but at low flow conditions, the correlation weakens.

Acknowledgments

This research was sponsored by the Air Force Office of Scientific Research and the NASA John H. Glenn Research Center at Lewis Field. This support is most gratefully acknowledged.

References

[1]Sherman, P., Dudley, R., and Suarez, M., "Blade-to-Blade Variability of the Pressure Associated with an Axial Compressor," American Society of Mechanical Engineers, ASME Paper 95-GT-442, June 1995.

[2]Sanders, A., and Fleeter, S., "Rotor Blade-to-Blade Wake Variability and Its Effect on Downstream Vane Response," *Journal of Propulsion and Power*, Vol. 18, No. 2, 2002, pp. 456–464.